CSF-1R inhibition alters macrophage polarization and blocks glioma progression

Stephanie M. Pyonteck[1,*], **Leila Akkari**[1,*], **Alberto J. Schuhmacher**[1,*], **Robert L. Bowman**[1], **Lisa Sevenich**[1], **Daniela F. Quail**[1], **Oakley C. Olson**[1], **Marsha L. Quick**[1], **Jason T. Huse**[3,4], **Virginia Teijeiro**[1], **Manu Setty**[2], **Christina S. Leslie**[2], **Yoko Oei**[5], **Alicia Pedraza**[3], **Jianan Zhang**[3,4], **Cameron W. Brennan**[3,4], **James C. Sutton**[5], **Eric C. Holland**[1,4], **Dylan Daniel**[5], and **Johanna A. Joyce**[1,4,#]

[1]Cancer Biology and Genetics, Memorial Sloan-Kettering Cancer Center, New York, NY 10065

[2]Computational Biology, Memorial Sloan-Kettering Cancer Center, New York, NY 10065

[3]Human Oncology and Pathogenesis Programs, Memorial Sloan-Kettering Cancer Center, New York, NY 10065

[4]Brain Tumor Center, Memorial Sloan-Kettering Cancer Center, New York, NY 10065

[5]Novartis Institutes for Biomedical Research, Emeryville, CA 94608, USA

Abstract

Glioblastoma multiforme (GBM) comprises several molecular subtypes including proneural GBM. Most therapeutic approaches targeting glioma cells have failed. An alternative strategy is to target cells in the glioma microenvironment, such as tumor-associated macrophages and microglia (TAMs). Macrophages depend upon colony stimulating factor (CSF)-1 for differentiation and survival. A CSF-1R inhibitor was used to target TAMs in a mouse proneural GBM model, which dramatically increased survival, and regressed established tumors. CSF-1R blockade additionally slowed intracranial growth of patient-derived glioma xenografts. Surprisingly, TAMs were not depleted in treated mice. Instead, glioma-secreted factors including GM-CSF and IFN-γ facilitated TAM survival in the context of CSF-1R inhibition. Alternatively activated/ M2 macrophage markers decreased in surviving TAMs, consistent with impaired tumor-promoting functions. These gene signatures were associated with enhanced survival in proneural GBM patients. Our results identify TAMs as a promising therapeutic target for proneural gliomas, and establish the translational potential of CSF-1R inhibition for GBM.

[#]Correspondence should be addressed to: joycej@mskcc.org.

[*]Indicates shared authorship

INTRODUCTION

GBM, the most aggressive form of glioma, has an invariably terminal prognosis, as patients respond minimally to current therapies, including surgery, radiation and chemotherapy[1]. One challenge in treating GBM is substantial tumor cell and genetic heterogeneity leading to aberrant activation of multiple signaling pathways[2,3]. Underscoring this heterogeneity is the identification of several GBM molecular subtypes, classified as proneural, neural, mesenchymal and classical[4]. In contrast, non-cancerous stromal cells in the tumor microenvironment represent genetically stable therapeutic targets[5,6]. TAMs in particular are associated with high tumor grade and poor prognosis in many cancers, including gliomas[7–9].

Several approaches have been used to ablate TAMs or inhibit their tumor-promoting functions in mouse models of cancer[10]. One strategy is CSF-1R inhibition, which depleted macrophages and reduced tumor volume in several xenografts[11,12]. A paracrine CSF-1/ EGF signaling loop was additionally implicated in breast cancer and glioma invasion[13,14]. Here we use a potent, selective CSF-1R inhibitor in multiple preclinical GBM models. These include RCAS-hPDGF-B/Nestin-Tv-a;*Ink4a/Arf*$^{-/-}$ transgenic mice[15,16], referred to as PDGF-B-driven gliomas (PDG), and intracranial xenografts of proneural GBM cell lines or patient-derived tumor spheres. We find that CSF-1R inhibition blocks glioma growth and progression through an unexpected mechanism by which TAMs are not depleted, but instead 're-educated' within the glioma microenvironment.

RESULTS

Macrophages accumulate in a mouse model of gliomagenesis and can be targeted by CSF-1R inhibition

In PDG mice, Nestin$^+$ glial progenitors express the RCAS virus receptor, Tv-a, enabling specific delivery of the initiating oncogene, PDGF-B. PDG tumorigenesis recapitulates pathological and molecular features of human proneural GBM[4,17–19]. We first investigated whether macrophages accumulate as in human gliomas[8,9]. Indeed, CD11b$^+$ myeloid cells/ macrophages were significantly increased in PDG GBM compared to normal brain, and *Cd68, Csf-1* and *Csf-1r* mRNA expression was elevated (Supplementary Fig. 1a, b). Glioma cells and TAMs express *Csf-1*, while *Csf-1r* is only expressed in TAMs (Fig. 1a, b, Supplementary Fig. 1c–e).

BLZ945 is a brain-penetrant CSF-1R inhibitor (Supplementary Fig. 2a, Supplementary Methods). The biochemical IC$_{50}$ for CSF-1R is 1nM, which is >3200-fold higher than its affinity for other kinases (Supplementary Table 1). Treatment of bone marrow-derived macrophages (BMDMs) with BLZ945 inhibited CSF-1-dependent proliferation (EC$_{50}$=67nM), and decreased CSF-1R phosphorylation, similar to CSF-1R antibody blockade (Fig. 1c, Supplementary Fig. 2b–d). BLZ945 also reduced viability of CRL-2467 microglia, *Ink4a/Arf*$^{-/-}$ BMDMs (PDG genetic background), and NOD/SCID BMDMs (Supplementary Fig. 3a–c). Importantly, BLZ945 treatment in culture did not affect proliferation of any PDG-derived tumor cell lines (all *Csf-1r*-negative), or U-87 MG human glioma cells, and PDG cell tumor sphere formation was unaffected (Fig. 1d, Supplementary

Fig. 3d–g). Thus, BLZ945 has no direct effects on glioma cells, and perturbs macrophage survival through CSF-1R inhibition.

CSF-1R inhibition blocks glioma progression and significantly improves survival

We next assessed BLZ945 in PDG preclinical trials. At 2.5 weeks post-glioma initiation, 30% of animals had small tumors (grade II or III), and 70% had no tumor by histology or MRI (Supplementary Fig. 4a, b). Mice were treated with BLZ945 or vehicle, and evaluated for symptom-free survival (Fig. 1e). Median survival in the vehicle-treated cohort was 5.7 weeks. In striking contrast, BLZ945 significantly improved long-term survival with 64.3% surviving to the 26-week trial endpoint (Fig. 1f). This endpoint was chosen because *Ink4a/Arf*^{-/-} mice develop spontaneous tumors, including lymphomas and sarcomas, beginning at ~30 weeks[20]. BLZ945 was well-tolerated over long-term treatment, with no visible side-effects (Supplementary Fig. 4e), consistent with histopathological studies[21]. Histological grading revealed high-grade, invasive gliomas in all vehicle-treated mice. By contrast, BLZ945-treated animals had significantly less-malignant tumors, and no detectable lesions in 55.6% of asymptomatic mice at the endpoint (Fig. 1g, Supplementary Fig. 4c, d, f).

We then monitored the effects of BLZ945 on established high-grade PDG tumors, which are histologically similar to human GBMs at time of diagnosis[17]. We performed a 7-day trial incorporating MRI to assess initial tumor volume and subsequent growth (Fig. 2a). PDG mice with detectable tumors were randomized into BLZ945 or vehicle cohorts. In the vehicle group, tumor growth increased substantially. By contrast, BLZ945 halted glioma growth, and the majority of tumors decreased in size (Fig. 2b, d, e, Supplementary Fig. 5a, b). A third cohort of mice with large gliomas was treated with BLZ945 (denoted 'BLZ945 large'), and the vast majority showed regression (Fig. 2c–e, Supplementary Fig. 5c). Comparison with a size-matched vehicle cohort was not possible, as most of those mice would not have survived to the trial endpoint. Inhibition of CSF-1R phosphorylation was confirmed in BLZ945-treated tumors, and hPDGF-B production by glioma cells was unaffected (Supplementary Fig. 6).

Since we used a PDGF-driven model for these initial trials, we wanted to exclude possible off-target effects of BLZ945 on glioma PDGFR signaling. Glioma cells express PDGFR-α and pericytes express PDGFR-β (Supplementary Fig. 7a, b). PDGFR inhibition reduces U-87 MG cell viability[22,23]. PDG tumors were modestly responsive to PDGFR inhibition *in vivo*[24] and in culture (Supplementary Fig. 7c). The affinity of BLZ945 for PDGFR-α is approximately 10,000-fold lower than for CSF-1R (Supplementary Table 1). Unlike PDGFR inhibitors, BLZ945 or an anti-CSF-1R antibody did not affect viability of U-87 MG and PDG cell lines (Fig. 1d, Supplementary Figs. 3d–e, 7c). Collectively, these data establish that the therapeutic effects of BLZ945 *in vivo* are via CSF-1R inhibition, not through off-target inhibition of PDGFR.

Multiple hallmarks of cancer are altered by CSF-1R blockade

To determine the mechanisms underlying the striking response to CSF-1R inhibition in established gliomas, we investigated multiple hallmarks of cancer[25] (Supplementary Table

2). Analyses were performed on tissues from the 7-day BLZ945 trial, including the midpoint (3d) and endpoint (7d) to capture dynamic effects of CSF-1R inhibition. While all vehicle-treated mice had high-grade gliomas, BLZ945-treated animals exhibited a pronounced histological response, characterized by tumor cell depopulation (Fig. 3a, Supplementary Fig. 8a). Correspondingly, glioma cell number within the region of the original tumor decreased dramatically (Fig. 3b–d).

Proliferation analyses revealed a 67–98% reduction following BLZ945 treatment (Fig. 3b, e). In addition, apoptosis increased by 9- to 17-fold after 3 days (Fig. 3b, f), and tumor vascularity decreased. This reduction was likely not due to direct effects of BLZ945 on endothelial cells, as their viability was unaffected in culture (Supplementary Fig. 8b–f). Thus, CSF-1R inhibition effectively reduces the growth and malignancy of gliomas through a combined effect of blocking cell proliferation and increasing apoptosis.

CSF-1R inhibition slows intracranial growth of human proneural GBM tumor spheres and cell lines

We next asked if CSF-1R inhibition was effective in experimental models of human proneural GBM, including primary tumor spheres (TS573, TS1137) and established cell lines (U251, LN229) (Supplementary Table 3 and Supplementary Methods respectively). The tumor spheres/ cell lines were either negative for *CSF-1R*, or showed negligible mRNA levels compared to the human macrophage line THP-1, and none were sensitive to BLZ945 in monoculture (Fig. 4a, b, Supplementary Fig. 9a, b).

We intracranially injected the glioma tumor sphere/ cell lines, and treated established tumors with either vehicle or BLZ945. All four human lines responded to BLZ945 *in vivo*, showing a clear histological response, and significantly reduced tumor growth and invasion (Fig. 4c–f, Supplementary Fig. 9c–e). Collectively, these results demonstrate the compelling preclinical efficacy of CSF-1R inhibition across multiple proneural GBM models, including genetically engineered mice and human-derived xenografts.

CSF-1R inhibition does not affect TAM numbers in treated tumors due to presence of glioma-supplied survival factors

Macrophage survival depends on CSF-1R signaling[26], and thus we expected CSF-1R inhibition to deplete macrophages. Indeed, BLZ945 treatment reduced CD11b$^+$Ly6G$^-$ cells in blood. Microglia numbers in normal brains were substantially decreased by BLZ945; surprisingly, however, CSF-1R inhibition did not affect TAM numbers in PDG gliomas, compared to vehicle (Fig. 5a, b, Supplementary Figs. 10, 11). Similar results were observed in human tumor sphere and cell line xenografts (Supplementary Fig. 12a, b).

BLZ945-treated TAMs retained CSF-1R expression *in vivo*, and there were no significant differences compared to vehicle-treated PDG gliomas (Supplementary Fig. 13a). We examined whether relative proportions of resident microglia and recruited BMDMs were altered in the PDG model. We performed BM transplantation experiments using GFP$^+$ BM, and initiated gliomas following confirmation of BM reconstitution (Supplementary Fig. 13b, c). The proportion of GFP$^+$CD68$^+$ macrophages was unchanged following BLZ945

treatment (Supplementary Fig. 13d), indicating no evident alteration in peripheral recruitment. We evaluated additional strategies used to deplete macrophages in other tumor types or the brain, and similarly found that while macrophages in peripheral tissues or normal brain decreased, there was no effect on TAM numbers in PDG tumors (Supplementary Fig. 14). We analyzed other immune cell types in gliomas following BLZ945 treatment and found no significant differences in cell numbers (Supplementary Fig. 13e). Finally, given varying reports of CSF-1R expression by neurons[27,28], we examined neuron numbers in gliomas or normal brain and found no differences following BLZ945 (Supplementary Fig. 13f), consistent with our detection of CSF-1R only in macrophages (Supplementary Fig. 1c–e).

To explore the mechanisms whereby glioma TAMs were specifically protected from BLZ945-induced apoptosis, we investigated if glioma-supplied factors supported macrophage survival in the presence of CSF-1R inhibition. Indeed, glioma cell-conditioned media (GCM) from PDG or human cell lines protected BMDMs from death induced by BLZ945 (Fig. 5c, Supplementary Figs. 12c, 15a, b). This was analogous to TAM maintenance observed for all models *in vivo*, and also indicated the survival factors were secreted. We screened GCM from a panel of PDG cell lines and identified multiple protective lines and one non-protective line (Supplementary Fig. 16a). By comparing the protective versus non-protective GCM using antibody arrays, we identified differentially secreted proteins (Supplementary Fig. 16b, c), which were tested in parallel with known macrophage survival factors[29]. From this screen, we identified three cytokines that promoted the survival and/or proliferation of BMDMs in the presence of BLZ945: GM-CSF/CSF-2, IFN-γ and CXCL10 (Fig. 5d, e, Supplementary Figs. 17, 18a–d). Critically, when these factors were added in combination to GCM from the non-protective line, this conferred BMDM protection from BLZ945-induced killing (Supplementary Fig. 18e), in association with elevated Akt activation in macrophages, similar to treatment with GCM from protective lines (Fig. 5f, g). Consistent with their protective effect, expression of these cytokines and their receptors were substantially elevated in PDG gliomas compared to normal brain, and interestingly were also produced by TAMs themselves (Supplementary Fig. 19). These results establish that glioma-supplied factors promote TAM survival in the presence of a CSF-1R inhibitor.

CSF-1R inhibition reduces M2 macrophage polarization in treated gliomas

We next asked how CSF-1R inhibition elicited such a potent anti-tumor response *in vivo*, despite no evident TAM depletion. We hypothesized that TAMs from CSF-1R inhibitor-treated animals were functionally altered, and used microarray expression profiling of TAMs isolated from BLZ945- and vehicle-treated gliomas to identify 257 differentially expressed genes. 52 genes were significantly upregulated and 205 were downregulated; denoted as the 'total' gene signature (Fig. 6a, Supplementary Fig. 20a, b, Supplementary Table 4). CSF-1R inhibition in BLZ945-treated TAMs was corroborated by downregulation of Egr2 targets, a transcription factor downstream of CSF-1R[30] (Supplementary Fig. 20c). To determine the minimal set of genes that discriminated treatment groups we employed a lasso logistic regression model[31] (see Online Methods). This identified a 5-gene signature for BLZ945 treatment: adrenomedullin (*Adm*), arginase 1 (*Arg1*), clotting factor *F13a1*,

mannose receptor C type 1 (*Mrc1/CD206*), protease inhibitor *serpinb2/PAI2* (Fig. 6b; denoted 'minimal' gene signature). Of these, 4 were downregulated following BLZ945 treatment. qPCR analyses on whole gliomas and sorted cell populations confirmed these findings (Supplementary Fig. 20d, e). *Serpinb2*, the only upregulated gene in the minimal signature, correlates positively with increased survival in breast cancer[32]. Interestingly, each of the downregulated genes has been associated with alternatively activated/ M2 macrophage polarization[33–38] (Supplementary Table 4).

In many tumors, TAMs are M2 polarized, which is associated with pro-tumorigenic functions[39]. Further, macrophages in human gliomas exhibit an M2-like phenotype, correlated with higher tumor grade[9]. Given the striking M2 gene enrichment in the minimal signature, we examined the total gene list to determine if other M2-associated markers were similarly downregulated by BLZ945, which revealed 5 additional genes (Supplementary Fig. 20f, Supplementary Table 4). Apart from IL-1β, classically activated/ M1 genes were not correspondingly upregulated (Supplementary Fig. 20g). Interestingly, CSF-1 favors M2 macrophage polarization in culture[40,41], consistent with our finding that BLZ945 reduces M2 gene expression *in vivo*.

To explore how glioma cells and CSF-1R inhibition regulate M2 macrophage polarization we used cell-based assays, and exposed BMDMs to GCM to model microenvironmental interactions. Expression of all nine differentially expressed M2 genes (Supplementary Fig. 20f) significantly increased, and was reversed by BLZ945 (Fig. 6c). Analysis of a subset of these genes in microglia cell lines, BV-2 and CRL-2467, showed similar results (Supplementary Fig. 21a, b). We next examined Mrc1 levels in co-cultures and freshly isolated mouse glioma microenvironment cultures containing TAMs. Mrc1 was selected as a well-established M2 flow cytometry marker, facilitating determination of its macrophage-specific expression in mixed cultures. Mrc1 also decreased in response to BLZ945 (Fig. 6d, Supplementary Fig. 21c, d), paralleling its downregulation *in vivo*.

Interestingly, human glioma CM suppressed macrophage phagocytosis *in vitro* in conjunction with M2 polarization[42]. To determine whether BLZ945 altered macrophage phagocytosis *in vivo*, tissues were co-stained for the macrophage cell surface marker CD11b, the glioma cell marker Olig2 [43], and cleaved caspase 3 (CC3). Phagocytic capacity (number of CD11b+ macrophages that had engulfed Olig2+CC3+ glioma cells), increased 7.1-fold in the BLZ945 large group compared to vehicle (Supplementary Fig. 22, Supplementary Table 2). To control for glioma cell death, we analyzed phagocytic capacity post-irradiation, which increased 4-fold. Therefore, macrophages in BLZ945-treated gliomas undergo an increase in phagocytic function that is apparently not solely dependent on enhanced tumor apoptosis. Together, this suggests that following CSF-1R inhibition, glioma TAMs lose M2 polarization and show enhanced phagocytosis, providing a molecular corollary for their impaired tumor-promoting functions.

Heterotypic signaling between macrophages and glioma cells is abrogated by CSF-1R inhibition

As BLZ945 blocked PDG proliferation *in vivo*, we examined whether glioma cell proliferation was modulated by exposure to macrophages in cell culture, and if it was

reduced by CSF-1R inhibition. BMDMs were stimulated with GCM to mimic their 'education' in the glioma microenvironment (referred to hereafter as 'stimulated-BMDMs'), and subsequently added to glioma cells in co-culture (Supplementary Fig. 15a). Cell cycle analysis showed that co-culture of stimulated-BMDMs with PDG cells significantly increased proliferation. Interestingly, this induction was abrogated by addition of BLZ945 or a CSF-1R antibody (Fig. 6e, Supplementary Fig. 15c), suggesting the M2-dependent nature of this effect.

We investigated whether macrophage-secreted factors influenced activation of known signaling effectors of proliferation/survival within glioma cells, including Akt and Erk. Levels of phosphorylated Akt (pAkt) in glioma cells increased in response to CM from the stimulated-BMDMs compared to naïve-BMDM CM. This induction was significantly abrogated when CM from stimulated-BMDMs was collected in the presence of BLZ945 (Fig. 6f, Supplementary Fig. 23a, b). pErk levels in glioma cells did not change during this time course (Fig. 6f). Addition of the Akt inhibitor MK2206 significantly impaired the macrophage CM-induced proliferation of glioma cells (Supplementary Fig. 23c), implicating this pathway as an important driver of signaling in the GBM microenvironment. We also investigated whether macrophages promoted glioma cell proliferation *in vivo* by orthotopically co-injecting BMDMs + PDG cells, or PDG cells alone. Interestingly, co-injection of macrophages with glioma cells enhanced tumor growth by 62% compared to glioma cells alone, and this induction was blocked by BLZ945 treatment (Supplementary Fig. 23d, $P<0.05$). Collectively, these data demonstrate that macrophages and glioma cells have reciprocal effects on the survival, proliferation and/ or polarization of each other to promote tumorigenesis, and that this heterotypic signaling can be blocked by CSF-1R inhibition.

Gene signatures of CSF-1R inhibition predict survival advantage in proneural GBM

Finally, we examined whether BLZ945 gene signatures generated from mouse TAMs might have translational value through differential survival associations in individuals with GBM. We used the total gene signature to classify TCGA subjects[44] and a second combined series[45–47] into 'BLZ945-like' or 'Vehicle-like' classes. Interestingly, there was a proneural-specific increase in median survival for the 'BLZ945-like' class, ranging from 7.5–31.5 months (Supplementary Fig. 24a, b). We also used the minimal gene signature and observed that this markedly smaller gene set recapitulated the 'BLZ945-like' survival advantage in proneural subjects (Fig. 6g, h, Supplementary Fig. 24a–d, Supplementary Tables 5, 6). Notably, the survival increase was not evident in other GBM subtypes, and was independent of G-CIMP[+] status[48] (Supplementary Fig. 24e, Supplementary Table 7). To determine if the minimal gene signature predicted survival independent of macrophage number, we utilized expression of macrophage-specific genes (*AIF1, CD68, ITGAM*) as surrogates for macrophage number in a cox proportional hazards model (Supplementary Tables 8, 9). None of the macrophage-specific genes correlated with worse prognosis, indicating that the minimal gene signature of BLZ945 treatment is a subtype-specific, prognostic predictor of GBM patient survival that is independent of total macrophage number. This also suggests that the TAM phenotype within a tumor may predict overall survival better than TAM number *per se*. The subtype specificity for this survival difference is consistent with the

minimal and total gene signatures having been generated from the PDG model, which most closely represents proneural GBM[19].

DISCUSSION

We show here that a novel CSF-1R inhibitor blocks malignant progression, regresses established gliomas and dramatically enhances survival in a transgenic mouse model of proneural GBM. Moreover, multiple proneural GBM human xenografts responded similarly to CSF-1R inhibition, underscoring the therapeutic relevance of these findings. Surprisingly, we found that TAMs in all models were specifically protected from CSF-1R inhibitor-induced apoptosis. This contrasted with the observed depletion of microglia in the normal brain and macrophages in other tissues, consistent with previous reports [11,12]. This suggested that glioma-supplied factors facilitate TAM survival in the presence of BLZ945, while neighboring microglia outside of the tumor mass are not exposed to these protective signals and are thus depleted. Modeling these microenvironment-mediated effects in culture allowed us to screen and identify GM-CSF and IFN-γ as glioma-supplied factors that facilitate macrophage survival in the context of CSF-1R inhibition. Critically, expression of these factors, or their receptors, were enriched in gliomas compared to normal brain, consistent with their pro-survival functions. This led us to ask whether TAM functions were impaired following CSF-1R inhibition, given that their numbers were not altered. Indeed, expression analyses of surviving TAMs *in vivo* revealed a decrease in alternatively activated/ M2 macrophage markers, consistent with blunted tumor-promoting functions. Interestingly, we also modeled this phenomenon in culture, and demonstrated that induction of M2 polarization by glioma-secreted factors, and its reversal by CSF-1R inhibition, are both direct effects. Together, these data indicate that the presence of survival factors in the glioma microenvironment protects TAMs from CSF-1R inhibitor-mediated killing, enabling their 're-education' and an associated striking anti-tumor response.

There are several potential clinical implications of these findings. First, macrophage accumulation correlates with malignancy in human gliomas[8,9], supporting therapeutic targeting of TAMs. Second, we find that alteration of TAM tumor-promoting functions can significantly affect malignancy, and that depletion is not strictly necessary for effective macrophage-targeted therapy. Third, in light of our preclinical data in proneural human xenografts and mouse models, and the prognostic advantage associated with 'BLZ945-like' signatures in proneural subjects, it is possible that proneural GBMs are particularly dependent on the tumor-promoting functions of TAMs. As such, in future studies it will be interesting to determine whether other GBM subtypes respond similarly to CSF-1R inhibition. Fourth, myeloid cells, including macrophages, blunt chemotherapeutic response in breast cancer models[49,50] and promote re-vascularization following irradiation in GBM xenografts[51]. Thus, it may be instructive to consider CSF-1R inhibitors in combination with glioma cell-directed therapies, opening the possibility for synergistic effects.

In sum, this study uncovers a new therapeutic strategy for targeting cells in the glioma microenvironment. Rather than depleting stromal cells, as has been the goal with many microenvironment-targeted therapies to date, re-educating these cells has the potential to not

only abolish their pro-tumorigenic functions, but to actively enlist them as suppressors of tumorigenesis.

Supplementary Material

Refer to Web version on PubMed Central for supplementary material.

Acknowledgments

References

1. Stupp R, et al. Radiotherapy plus concomitant and adjuvant temozolomide for glioblastoma. N Engl J Med. 2005; 352:987–996. [PubMed: 15758009]

2. Wen PY, Kesari S. Malignant gliomas in adults. N Engl J Med. 2008; 359:492–507. [PubMed: 18669428]

3. Dunn GP, et al. Emerging insights into the molecular and cellular basis of glioblastoma. Genes Dev. 2012; 26:756–784. [PubMed: 22508724]

4. Verhaak RG, et al. Integrated genomic analysis identifies clinically relevant subtypes of glioblastoma characterized by abnormalities in PDGFRA, IDH1, EGFR, and NF1. Cancer Cell. 2010; 17:98–110. [PubMed: 20129251]

5. Balkwill FR, Mantovani A. Cancer-related inflammation: Common themes and therapeutic opportunities. Semin Cancer Biol. 2012; 22:33–40. [PubMed: 22210179]

6. Joyce JA, Pollard JW. Microenvironmental regulation of metastasis. Nat Rev Cancer. 2009; 9:239–252. [PubMed: 19279573]

7. Bingle L, Brown NJ, Lewis CE. The role of tumour-associated macrophages in tumour progression: implications for new anticancer therapies. J Pathol. 2002; 196:254–265. [PubMed: 11857487]

8. Hussain SF, et al. The role of human glioma-infiltrating microglia/macrophages in mediating antitumor immune responses. Neuro Oncol. 2006; 8:261–279. [PubMed: 16775224]

9. Komohara Y, Ohnishi K, Kuratsu J, Takeya M. Possible involvement of the M2 anti-inflammatory macrophage phenotype in growth of human gliomas. J Pathol. 2008; 216:15–24. [PubMed: 18553315]

10. Ruffell B, Affara NI, Coussens LM. Differential macrophage programming in the tumor microenvironment. Trends Immunol. 2012; 33:119–126. [PubMed: 22277903]

11. Manthey CL, et al. JNJ-28312141, a novel orally active colony-stimulating factor-1 receptor/FMS-related receptor tyrosine kinase-3 receptor tyrosine kinase inhibitor with potential utility in solid tumors, bone metastases, and acute myeloid leukemia. Mol Cancer Ther. 2009; 8:3151–3161. [PubMed: 19887542]

12. Patel S, Player MR. Colony-stimulating factor-1 receptor inhibitors for the treatment of cancer and inflammatory disease. Curr Top Med Chem. 2009; 9:599–610. [PubMed: 19689368]

13. Wyckoff J, et al. A paracrine loop between tumor cells and macrophages is required for tumor cell migration in mammary tumors. Cancer Res. 2004; 64:7022–7029. [PubMed: 15466195]

14. Coniglio SJ, et al. Microglial stimulation of glioblastoma invasion involves EGFR and CSF-1R signaling. Mol Med. 2012; 18:519–527. [PubMed: 22294205]

15. Fomchenko EI, et al. Recruited cells can become transformed and overtake PDGF-induced murine gliomas in vivo during tumor progression. PLoS One. 2011; 6:e20605. [PubMed: 21754979]

16. Hambardzumyan D, Amankulor NM, Helmy KY, Becher OJ, Holland EC. Modeling adult gliomas using RCAS/t-va technology. Transl Oncol. 2009; 2:89–95. [PubMed: 19412424]

17. Huse JT, Holland EC. Genetically engineered mouse models of brain cancer and the promise of preclinical testing. Brain Pathol. 2009; 19:132–143. [PubMed: 19076778]

18. Kennedy BC, et al. Dynamics of central and peripheral immunomodulation in a murine glioma model. BMC Immunol. 2009; 10:11. [PubMed: 19226468]

19. Hambardzumyan D, Parada LF, Holland EC, Charest A. Genetic modeling of gliomas in mice: new tools to tackle old problems. Glia. 2011; 59:1155–1168. [PubMed: 21305617]

20. Serrano M, et al. Role of the INK4a locus in tumor suppression and cell mortality. Cell. 1996; 85:27–37. [PubMed: 8620534]

21. Wang T, et al. Investigation of correlation among safety biomarkers in serum, histopathological examination, and toxicogenomics. Int J Toxicol. 2011; 30:300–312. [PubMed: 21653914]

22. Kilic T, et al. Intracranial inhibition of platelet-derived growth factor-mediated glioblastoma cell growth by an orally active kinase inhibitor of the 2-phenylaminopyrimidine class. Cancer Res. 2000; 60:5143–5150. [PubMed: 11016641]

23. Takeuchi H, Kanzawa T, Kondo Y, Kondo S. Inhibition of platelet-derived growth factor signalling induces autophagy in malignant glioma cells. Br J Cancer. 2004; 90:1069–1075. [PubMed: 14997209]

24. Shih AH, et al. Dose-dependent effects of platelet-derived growth factor-B on glial tumorigenesis. Cancer Res. 2004; 64:4783–4789. [PubMed: 15256447]

25. Hanahan D, Weinberg RA. Hallmarks of cancer: the next generation. Cell. 2011; 144:646–674. [PubMed: 21376230]

26. Chitu V, Stanley ER. Colony-stimulating factor-1 in immunity and inflammation. Curr Opin Immunol. 2006; 18:39–48. [PubMed: 16337366]

27. Luo J, et al. Colony-stimulating factor 1 receptor (CSF1R) signaling in injured neurons facilitates protection and survival. J Exp Med. 2013; 210:157–172. [PubMed: 23296467]

28. Erblich B, Zhu L, Etgen AM, Dobrenis K, Pollard JW. Absence of colony stimulation factor-1 receptor results in loss of microglia, disrupted brain development and olfactory deficits. PLoS One. 2011; 6:e26317. [PubMed: 22046273]

29. Lin H, et al. Discovery of a cytokine and its receptor by functional screening of the extracellular proteome. Science. 2008; 320:807–811. [PubMed: 18467591]

30. Bradley EW, Ruan MM, Oursler MJ. Novel pro-survival functions of the Kruppel-like transcription factor Egr2 in promotion of macrophage colony-stimulating factor-mediated osteoclast survival downstream of the MEK/ERK pathway. J Biol Chem. 2008; 283:8055–8064. [PubMed: 18198176]

31. Friedman J, Hastie T, Tibshirani R. Regularization paths for generalized linear models via coordinate descent. J Stat Software. 2010; 33:1–22.

32. Croucher DR, Saunders DN, Lobov S, Ranson M. Revisiting the biological roles of PAI2 (SERPINB2) in cancer. Nat Rev Cancer. 2008; 8:535–545. [PubMed: 18548086]

33. Biswas SK, Mantovani A. Macrophage plasticity and interaction with lymphocyte subsets: cancer as a paradigm. Nat Immunol. 2010; 11:889–896. [PubMed: 20856220]

34. Torocsik D, et al. Factor XIII-A is involved in the regulation of gene expression in alternatively activated human macrophages. Thromb Haemost. 2010; 104:709–717. [PubMed: 20664907]

35. Probst-Cousin S, Rickert CH, Gullotta F. Factor XIIIa-immunoreactivity in tumors of the central nervous system. Clin Neuropathol. 1998; 17:79–84. [PubMed: 9561329]

36. Chen P, et al. Tumor-associated macrophages promote angiogenesis and melanoma growth via adrenomedullin in a paracrine and autocrine manner. Clin Cancer Res. 2011; 17:7230–7239. [PubMed: 21994414]

37. Schroder WA, Major L, Suhrbier A. The role of SerpinB2 in immunity. Crit Rev Immunol. 2011; 31:15–30. [PubMed: 21395508]

38. Solinas G, et al. Tumor-conditioned macrophages secrete migration-stimulating factor: a new marker for M2-polarization, influencing tumor cell motility. J Immunol. 2010; 185:642–652. [PubMed: 20530259]

39. Sica A, Schioppa T, Mantovani A, Allavena P. Tumour-associated macrophages are a distinct M2 polarised population promoting tumour progression: potential targets of anti-cancer therapy. Eur J Cancer. 2006; 42:717–727. [PubMed: 16520032]

40. Fleetwood AJ, Lawrence T, Hamilton JA, Cook AD. Granulocyte-macrophage colony-stimulating factor (CSF) and macrophage CSF-dependent macrophage phenotypes display differences in cytokine profiles and transcription factor activities: implications for CSF blockade in inflammation. J Immunol. 2007; 178:5245–5252. [PubMed: 17404308]

41. Sierra-Filardi E, et al. Activin A skews macrophage polarization by promoting a proinflammatory phenotype and inhibiting the acquisition of anti-inflammatory macrophage markers. Blood. 2011; 117:5092–5101. [PubMed: 21389328]

42. Wu A, et al. Glioma cancer stem cells induce immunosuppressive macrophages/microglia. Neuro Oncol. 2010; 12:1113–1125. [PubMed: 20667896]

43. Squatrito M, et al. Loss of ATM/Chk2/p53 pathway components accelerates tumor development and contributes to radiation resistance in gliomas. Cancer Cell. 2010; 18:619–629. [PubMed: 21156285]

44. McLendon R, et al. Comprehensive genomic characterization defines human glioblastoma genes and core pathways. Nature. 2008; 455:1061–1068. [PubMed: 18772890]

45. Freije WA, et al. Gene expression profiling of gliomas strongly predicts survival. Cancer Res. 2004; 64:6503–6510. [PubMed: 15374961]

46. Phillips HS, et al. Molecular subclasses of high-grade glioma predict prognosis, delineate a pattern of disease progression, and resemble stages in neurogenesis. Cancer Cell. 2006; 9:157–173. [PubMed: 16530701]

47. Murat A, et al. Stem cell-related "self-renewal" signature and high epidermal growth factor receptor expression associated with resistance to concomitant chemoradiotherapy in glioblastoma. J Clin Oncol. 2008; 26:3015–3024. [PubMed: 18565887]

48. Noushmehr H, et al. Identification of a CpG island methylator phenotype that defines a distinct subgroup of glioma. Cancer Cell. 2010; 17:510–522. [PubMed: 20399149]

49. Denardo DG, et al. Leukocyte complexity predicts breast cancer survival and functionally regulates response to chemotherapy. Cancer Discovery. 2011; 1:54–67. [PubMed: 22039576]

50. Shree T, et al. Macrophages and cathepsin proteases blunt chemotherapeutic response in breast cancer. Genes Dev. 2011; 25:2465–2479. [PubMed: 22156207]

51. Kioi M, et al. Inhibition of vasculogenesis, but not angiogenesis, prevents the recurrence of glioblastoma after irradiation in mice. J Clin Invest. 2010; 120:694–705. [PubMed: 20179352]
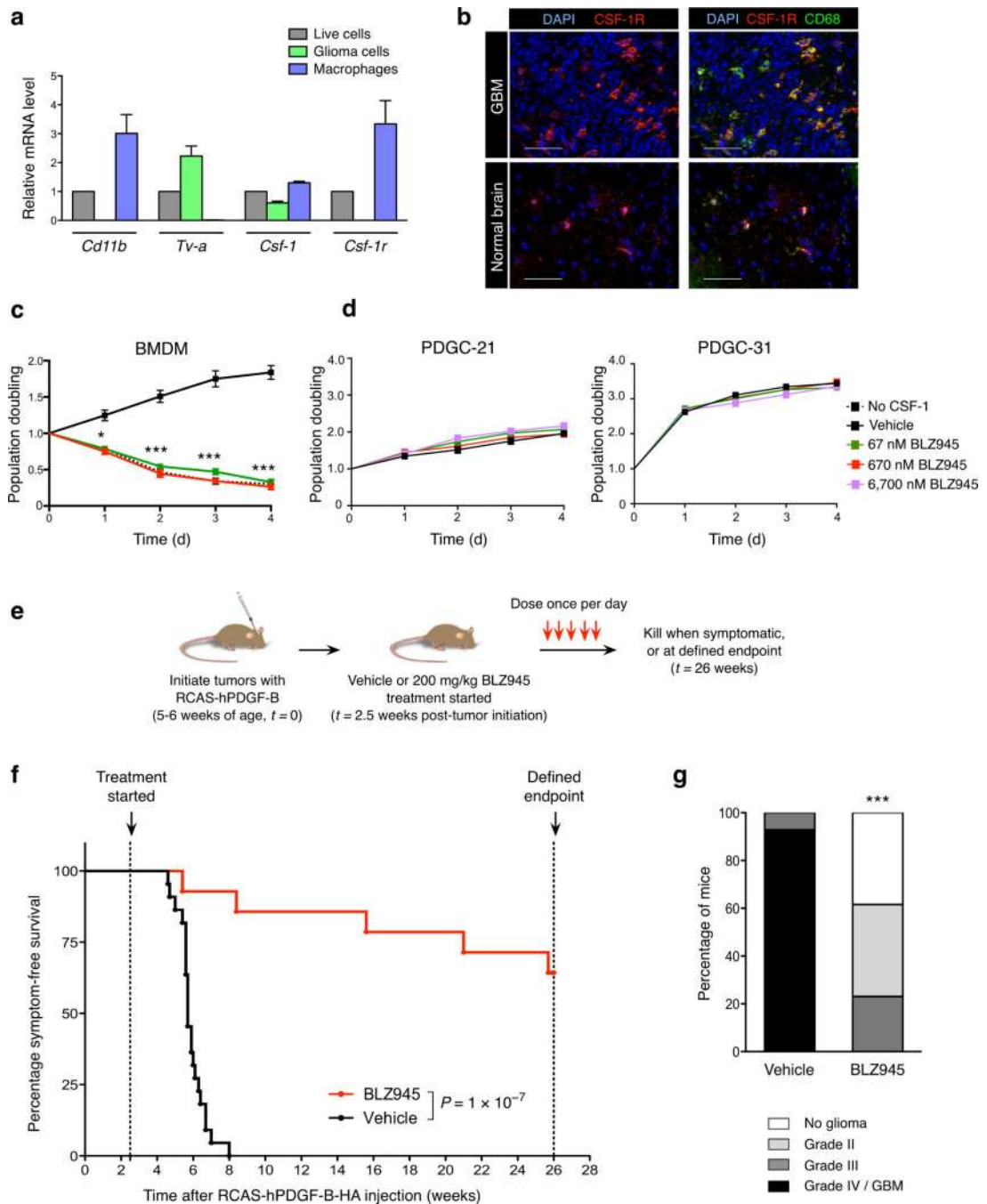
Figure 1. CSF-1R inhibition specifically targets macrophages, improves survival and decreases glioma malignancy in the transgenic PDG model

(**a**) Expression of *Csf-1* and *Csf-1r* in different cell populations from PDG-GFP gliomas: mixed population of live cells (DAPI−), purified glioma cells (GFP+) and macrophages (CD11b+Gr-1−). *Cd11b* and *Tv-a* were used as cell type-specific control genes for macrophages and glioma cells respectively. Expression is depicted relative to the live cell fraction, normalized to *Ubc* for each sample (*n* = 3). (**b**) Representative immunofluorescence images of normal brain or PDG GBM co-stained with CSF-1R, CD68 (macrophages/

microglia), and DAPI. Scale bar, 50 μm. **(c)** Graph showing the CSF-1R inhibitor BLZ945 blocked BMDM survival, with a comparable effect to CSF-1 deprivation, assessed by MTT assays; $n = 13$ independent replicates. **(d)** Graph showing MTT assays of BLZ945 treatment of independent PDGF-driven glioma cell (PDGC) primary lines derived from PDG mice (see also Supplementary Figs. 3d, 7c). Concentrations up to 6,700 nM BLZ945 (100× the dose required to effectively kill BMDMs *in vitro*) had no effect on glioma cell survival or proliferation, $n = 3$ independent replicates. **(e)** Experimental design for long-term survival trial: PDG mice were injected with RCAS-hPDGF-B-HA between 5–6 weeks of age to induce glioma formation, and randomly assigned to vehicle (20% captisol, $n = 22$) or BLZ945 (200 mg.kg^{-1}, $n = 14$) treatment groups at 2.5 weeks post-injection. Mice were dosed once daily until they developed symptoms or reached the trial endpoint, and **(f)** symptom-free survival curves generated. **(g)** Vehicle and BLZ945 groups were graded histologically ($n = 14$, 13 respectively). Graphs show mean and s.e.m. in (a, c–d). *P* values were obtained using unpaired two-tailed Student's t-test in (c–d), Log Rank (Mantel-Cox) test in (f), and Fisher's exact test in (g). *$P<0.05$, ***$P<0.001$.
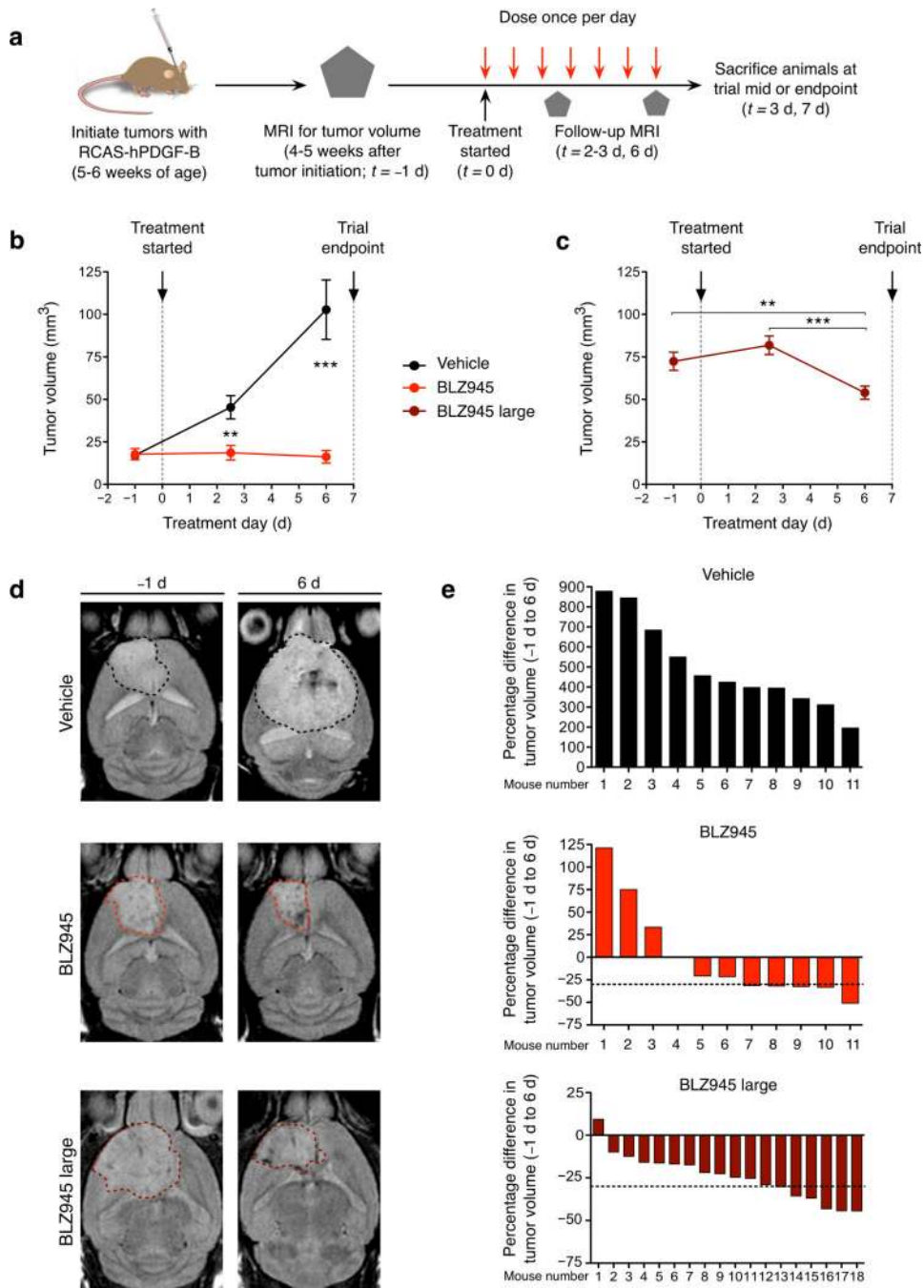
Figure 2. CSF-1R inhibition blocks tumor growth and effectively regresses established gliomas
(a) Experimental design for short-term 7d trial: PDG mice bearing detectable tumors by MRI were randomly assigned to vehicle or BLZ945 groups, with follow-up MRI as depicted. (b) Graph showing mean tumor volume over the time course for mice whose starting tumor volume was 4.5–40 mm^3 (vehicle or BLZ945, $n = 11$ per group) or (c) > 40 mm^3 (BLZ945 large, $n = 18$). (d) Representative images of T2-weighted MRI scans from the start and endpoint of the trial. Dashed line indicates region of interest used to calculate tumor volume. (e) Waterfall plots depicting change in tumor volume at endpoint relative to

starting tumor volume for each individual mouse. Horizontal dashed lines indicate a 30% decrease in tumor volume. In the vehicle group, there was a progressive, substantial increase in tumor growth, ranging from 195–879%. By contrast, in this short treatment period, 6 of 18 mice in the BLZ945 large group had >30% reduction in tumor volume, qualifying as a partial response according to Response Evaluation Criteria in Solid Tumors (RECIST). Graphs show mean ± s.e.m. *P* values were obtained using unpaired two-tailed Student's t-test; **P<0.01, ***P<0.001.
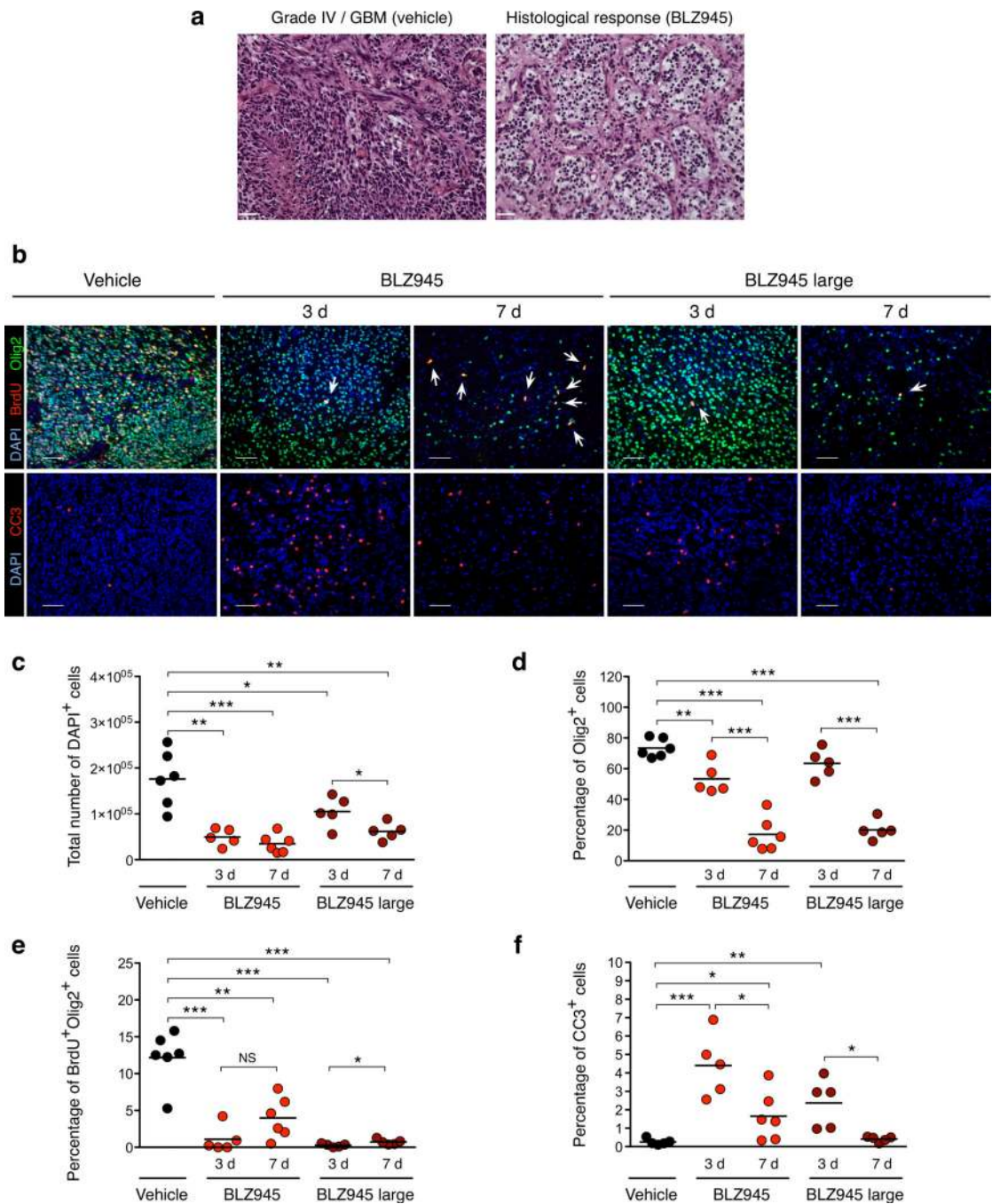
Figure 3. Short-term BLZ945 treatment results in reduced tumor grade and proliferation, and increased apoptosis

(a) Representative H&E images from 7d trial in the PDG model depicting grade IV/GBM (vehicle) and histological response (BLZ945). (b) Representative images from 3d and 7d timepoints stained for Olig2 (glioma cells), BrdU, cleaved caspase-3 (CC3), and DAPI. White arrows indicate rare BrdU+Olig2+ cells in BLZ945 groups. (c) Quantitation of total DAPI+ cells per tumor; (d) percentage of Olig2+ cells relative to total DAPI+ cells; (e) percentage of proliferating BrdU+Olig2+ cells relative to total DAPI+ cells; and (f)

percentage of apoptotic CC3^{+} cells relative to total DAPI^{+} cells ($n \geq 5$ per group). These analyses revealed a progressive reduction in cell number, and by 7d, average glioma cell density was reduced to ≤20% of total cells in both BLZ945 groups. Analysis of glioma cell proliferation revealed a 67–98% reduction following BLZ945 treatment. Circles represent individual mice and horizontal lines represent the mean. Scale bar, 50 μm. *P* values were obtained using unpaired two-tailed Student's t-test; NS=not significant, *$P<0.05$, **$P<0.01$, ***$P<0.001$.
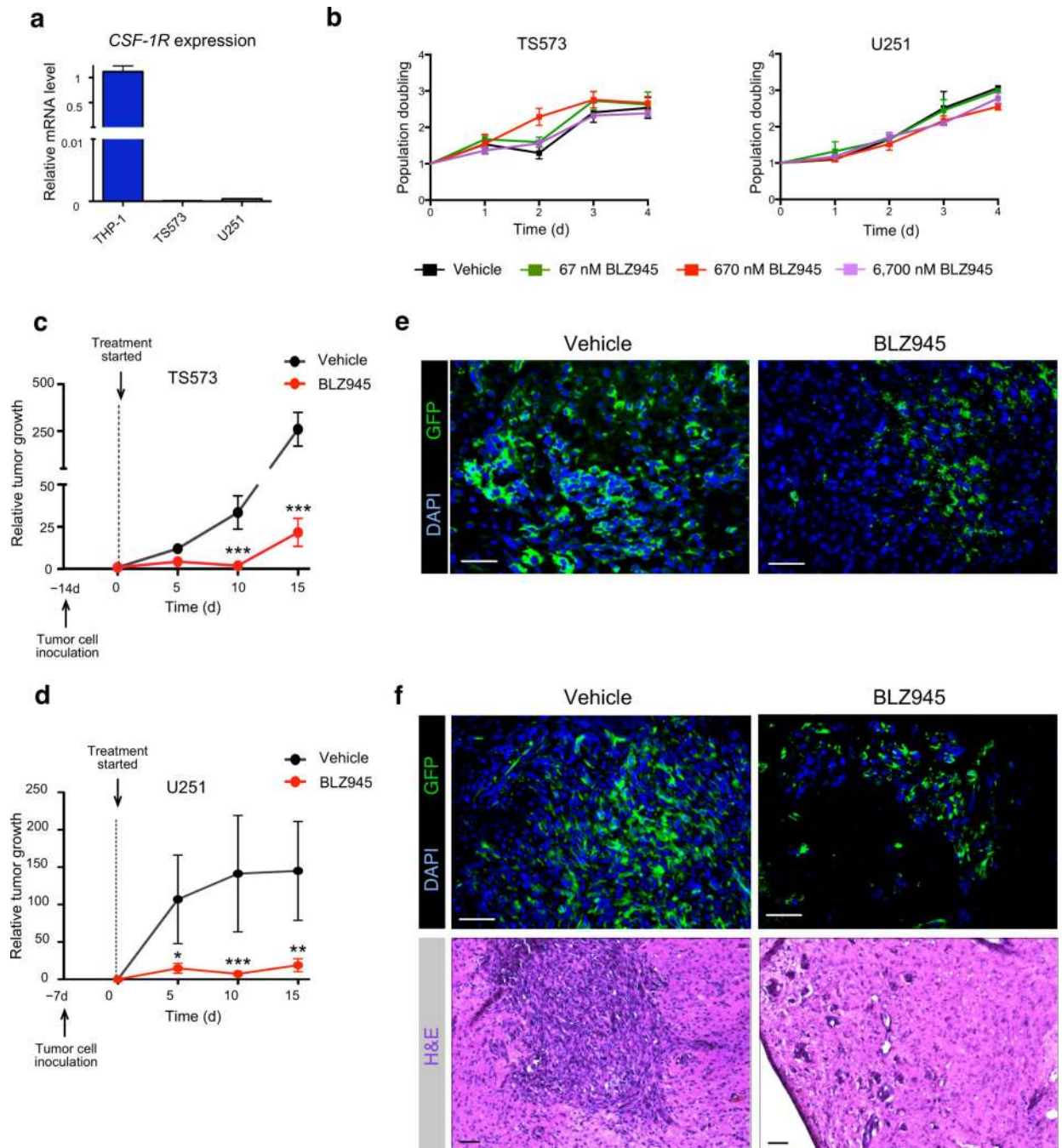
Figure 4. BLZ945 inhibits orthotopic tumor growth of patient-derived proneural tumor spheres and cell lines *in vivo*

(**a**) Graph shows assessment of *CSF-1R* mRNA expression in human proneural tumor sphere cells, TS573, and in the human proneural cell line, U251, compared to the human macrophage line THP-1 (positive control). Expression is normalized to *β2M* for each sample, *n* = 3 independent replicates. (**b**) Graph showing MTT assays of BLZ945 tested against TS573 and U251 human glioma cells, demonstrating no effect of BLZ945 concentrations up to 6,700 nM. *n* = 3 independent replicates. (**c, d**) Graphs showing relative

tumor growth determined by bioluminescence imaging (BLI) output in NOD/SCID mice intracranially injected with (c) 5×10^4 TS573 cells or (d) 2.5×10^5 U251 cells. Treatment with BLZ945 was initiated when tumors were in a positive growth phase determined by BLI, which corresponded to d14 for TS573 and d7 for U251. Mice were randomly assigned to vehicle ($n = 12$ for TS573, $n = 16$ for U251) or BLZ945 ($n = 11$ for TS573, $n = 17$ for U251) treatment groups. Tumor growth was evaluated every 5d for 15d, at which point vehicle-treated mice became symptomatic and both cohorts were sacrificed for further analyses. **(e, f)** Representative images of vehicle-treated and BLZ945-treated (e) TS573 and (f) U251 xenograft tumors described in (c, d), stained for GFP (tumor cells) and DAPI. Representative H&E images of both treatment groups for U251 xenografts are shown in the lower panels. Scale bar, 50 μm. Graphs represent mean and s.e.m. P values were obtained using nonparametric two-tailed Mann Whitney test; *P<0.05, **P<0.01, ***P<0.001.
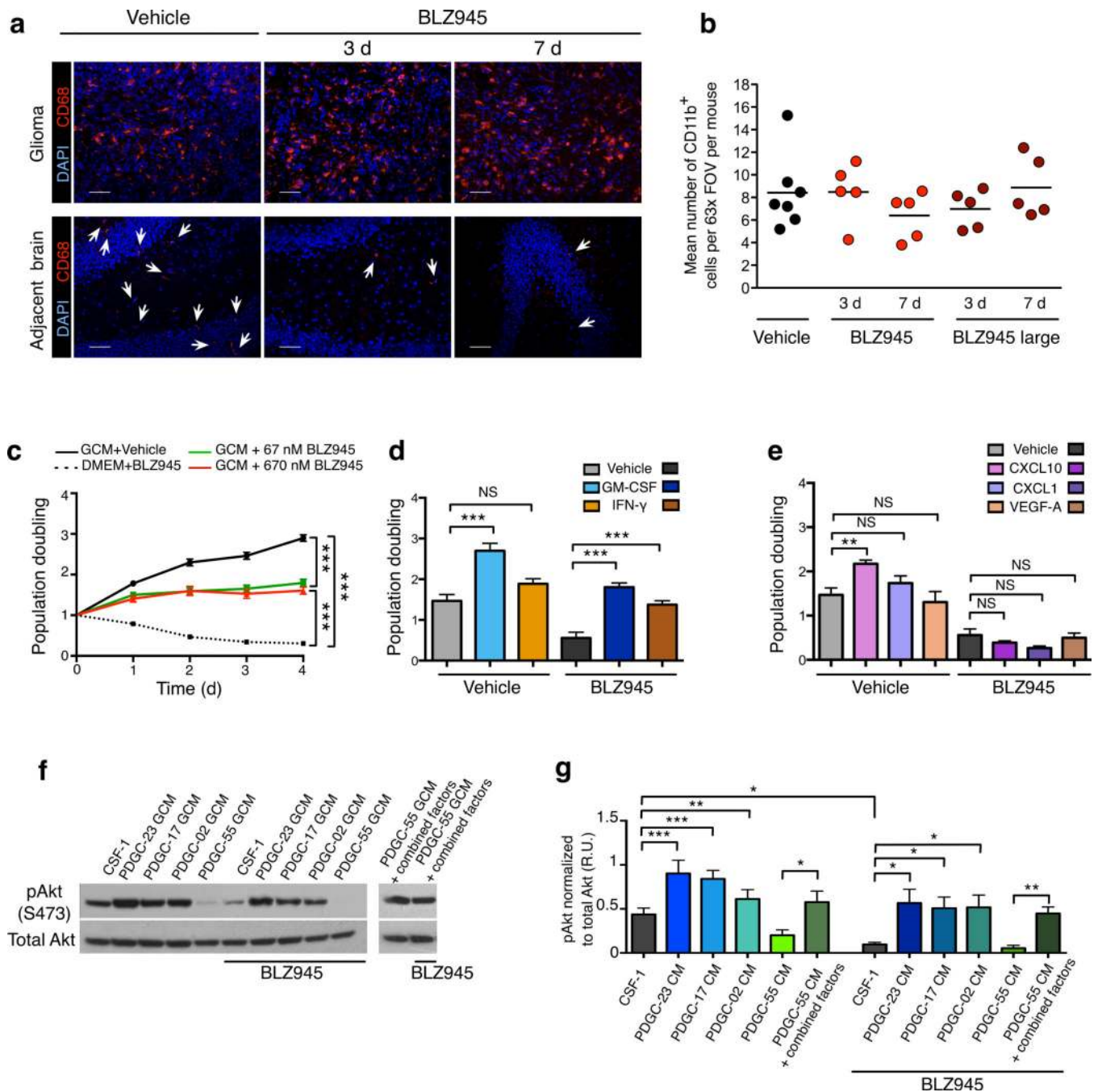
Figure 5. CSF-1R inhibition depletes normal microglia, but not TAMs in treated PDG gliomas due to the production of glioma-supplied survival factors

(a) Representative images of PDG gliomas (upper panel) and adjacent normal brain from the contralateral hemisphere of tumor-bearing mice (lower panel) from the 7d BLZ945 trial stained for CD68 and DAPI. (b) Graph showing quantitation of the mean number of CD11b^{+} macrophages per 63× field of view (FOV) within each mouse tumor at 7d. (c) Graph showing MTT assays of BMDMs, demonstrating that glioma cell-conditioned media (GCM) induced BMDM proliferation and protected BMDMs from BLZ945-induced apoptosis, $n = 19$ independent replicates. For comparison, BMDMs were cultured in non-

conditioned media supplemented with CSF-1. **(d)** Results compiled from MTT assays demonstrating that GM-CSF and IFN-γ individually protected BMDMs against BLZ945-induced death (n = 9 independent replicates) while **(e)** CXCL10 promoted proliferation (n = 6 independent replicates). These effects were not reproduced by other candidate factors, e.g. CXCL1 and VEGF-A shown here and in Supplementary Fig. 17. **(f)** Western blots showing activation of Akt (Ser473 phosphorylation site) in BMDMs. BMDMs were stimulated with freshly prepared GCM from protective (PDGC-23, PDGC-17, PDGC-02) or non-protective (PDGC-55) cell lines +/− BLZ945. In addition, GCM from non-protective PDGC-55 cells was supplemented with survival factors (GM-CSF, IFN-γ and CXCL10) +/− BLZ945. **(g)** Graph showing quantitation of phosphorylated Akt (pAkt), normalized to total Akt, demonstrating significant changes in pAkt levels between BMDMs stimulated with the protective or non-protective GCM +/− BLZ945. n = 4 independent replicates. BLZ945 was used at 670 nM in all cell culture assays unless otherwise specified. Circles in graph (b) represent individual mice (n ≥5 per group), and horizontal lines represent the mean. Data in other graphs represent mean and s.e.m. P values were obtained using unpaired two-tailed Student's t-test; NS = not significant, *P<0.05, **P<0.01, ***P<0.001. There were no significant differences for any comparisons in (b).
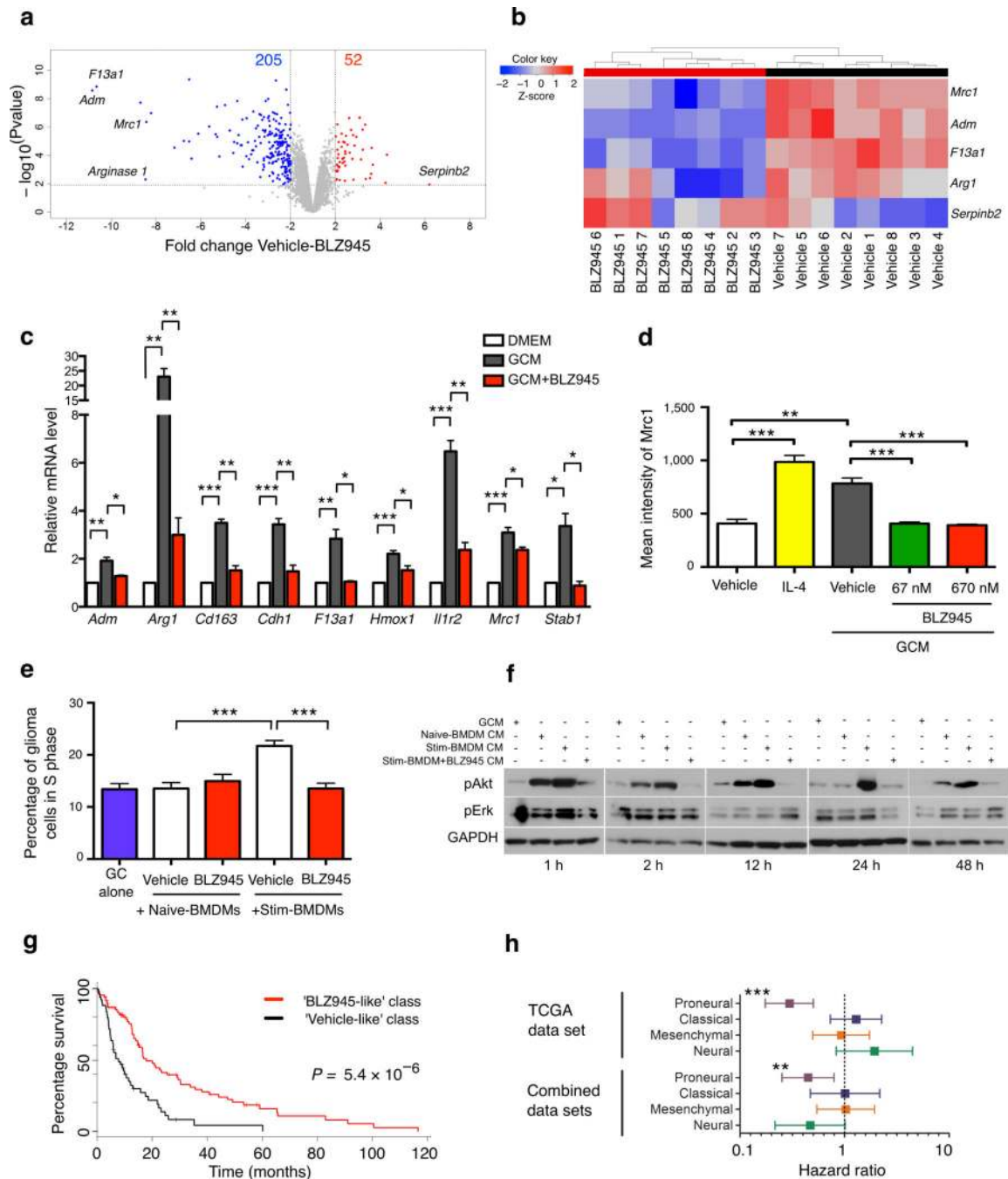
Figure 6. CSF-1R inhibition impairs heterotypic signaling between macrophages and glioma cells, and is predictive of improved survival in proneural GBM patients

(a) Volcano plot showing 257 differentially expressed genes in TAMs from BLZ945-treated mice compared to TAMs from vehicle controls (7d treatment, $n = 8$ each), termed the 'total' gene signature. 205 downregulated and 52 upregulated genes were differentially expressed in TAMs in the BLZ945 group. **(b)** Heatmap of the 'minimal' gene signature determined using a lasso logistic regression model trained on expression data in (a). This identified 5 genes, which when considered together, accurately differentiated between BLZ945 and

vehicle groups. **(c, d)** Graph showing expression of M2-associated genes in cultured BMDMs, demonstrating an increase with exposure to GCM, that was blocked in the presence of BLZ945, as determined by (c) qPCR for a panel of M2-associated genes identified in the total gene signature (Supplementary Fig. 20f) or (d) flow cytometry for Mrc1, $n = 7$ independent replicates. **(e)** Graph showing glioma cell cycle analyses, in which glioma cells were co-cultured with either naïve-BMDMs or stimulated-BMDMs (i.e. treated with GCM prior to co-culture, as shown in Supplementary Fig. 15a). Co-cultures were treated with BLZ945 or vehicle, and subjected to flow cytometric analyses, $n = 8$ independent replicates. **(f)** Western blots showing pAkt (Ser473) and pErk (Thr202/Tyr204) levels in glioma cells at the time points indicated. Glioma cells were exposed to CM produced by naïve- or stimulated-BMDMs +/− BLZ945; see schematic in Supplementary Fig. 23a. BLZ945 was used at 670 nM in all cell culture assays unless otherwise specified. **(g)** TCGA proneural patients were classified into 'BLZ945-like' and 'Vehicle-like' classes using the minimal gene signature from (b) (see Supplementary Methods). Patients classified as 'BLZ945-like' showed increased median survival of 10 months. **(h)** Hazard ratios (HR) and 95% confidence intervals (CI) for the minimal gene signature were determined for each subtype of TCGA and Combined datasets: HRs with a CI that does not cross 1.0 are considered significant. Graphs show mean and s.e.m. P values were obtained using unpaired two-tailed Student's t-test in (c–e), Log Rank test in (g), and Wald's test in (h). *$P<0.05$, **$P<0.01$, ***$P<0.001$.